Dalton Transactions

ROYAL SOCIETY OF CHEMISTRY

PAPER

View Article Online
View Journal | View Issue

Check for updates

Cite this: *Dalton Trans.*, 2025, **54**, 10343

Unprecedented photochromism of ferrocene-aryl dicyanovinylenes†

Atul Babasaheb Nipate and M. Rajeswara Rao *

Received 27th March 2025,
Accepted 2nd June 2025

DOI: 10.1039/d5dt00742a

rsc.li/dalton

An unprecedented photochromism of dicyanovinylene-functionalised ferrocenes has been explored. Photochromic systems (**M1–M3**) have been developed by the Knoevenagel condensation of dicyanovinylmethyl ferrocene with various aromatic aldehydes. **M1–M3** exhibit strong donor–acceptor interactions leading to intramolecular charge transfer in the ground state. As a result, the compounds exhibit intense colours and strong visible light absorption (λ_{abs1} = 362–485 nm, λ_{abs2} = 590–600 nm). The ferrocene systems (**M1–M3**) exhibit photochromism in the solution state when irradiated with ultraviolet light, with a high-contrast visual colour change from blue, yellow and green to yellow, purple and yellow, respectively. The process is reversible and takes place either by chemical or electrochemical reduction. In addition, **M2** exhibits turn-on fluorescence upon light irradiation, with a strong emission signal appearing in the red region (λ_{max} = 675 nm). This transformation is rapid and turns on fluorescence within 200 s. The photochromic behaviour of **M1–M3** has been ascribed to an unprecedented light-induced oxidation of ferrocene to ferrocenium, supported by EPR, NMR and FT-IR studies. This study is highly novel, and ferrocene-based systems have never been explored before for redox-switching-based photochromism.

Introduction

Photoresponsive materials that exhibit a change in their properties in response to photoirradiation are of paramount interest and possess important technological applications.[1–3] Photochromism is one of the properties of photoresponsive materials that studies molecules' reversible colour change behaviour upon light irradiation *via* reversible structural transformation.[4,5] Photochromic molecules have significant applications, including sunglasses,[6] optical data storage,[7,8] optoelectronic devices,[9] multifunctional smart materials,[10–15] super-resolution microscopy,[16] light-activated medicine,[17,18] *etc*. Various photochromic materials spanning inorganic[19] [$BaMgSiO_4$, $Y_3Al_2Ga_3O_{12}$, WO_3, TiO_2, MoO_3, AgCl, CaF_2: Ce, CaF_2: Gd] and organic (azobenzene, stilbene, spiropyran, diarylethene, hydrazone, *etc*.)[11,20–22] have been explored (Chart 1). Inorganic photochromic materials function *via* a change in the metal ion oxidation state, while their organic counterparts rely on structural transformation/isomerization. The inorganic materials possess high thermal stability and long cycling life but suffer from limited colour change and diversity; on the other hand, their organic counterparts possess a large diversity and high flexibility but have the limitations of poor thermal stability, slow colouration, and complex synthetic procedures. Thus, developing photochromic materials that possess the benefits of both organic and inorganic systems is key.

Ferrocene [$Fe(C_5H_5)_2$≡Fc] is a well-known organometallic compound for its outstanding redox properties and chemical stability.[23–25] Relying on the stable redox states of Fc, a library of Fc derivatives has been developed and explored for various applications, including catalysis, sensors, redox-active supramolecular switches, drug delivery, photonics, *etc*.[26] Despite the vast utility, Fc-based systems have never been explored for photochromic applications. Although a few examples of Fc-integrated photoresponsive azobenzene (AB), spiropyran (SP), diarylethene (DAE), *etc*., have been studied for photochromism,[27,28] these systems function through the structural transformation of the latter units. So far, no examples demonstrate the photochromic properties of Fc-based systems solely based on the redox-switching properties of Fc. Photochromic studies based on such transformation will be highly novel and open a new direction in this field, where the advantages of both organic and inorganic systems can be availed. Notably, Fc systems have previously been demonstrated as photosensitizers in solar cells[29] and photo-initiators for polymerization reactions,[30] where Fc will oxidize to ferrocenium (Fc^+) under light irradiation. This study provided an impetus for us to develop ferrocene-based photochromic systems.

Here, we report a novel class of Fc-based aryl dicyanovinylenes ($\mathbf{M_1}$–$\mathbf{M_3}$) that exhibit photochromic behaviour. The strong D–A interactions in $\mathbf{M_1}$–$\mathbf{M_3}$ render intense colour and

Department of Chemistry, IIT Dharwad, Dharwad-580011, Karnataka, India.
E-mail: rajesh@iitdh.ac.in

† Electronic supplementary information (ESI) available. See DOI: https://doi.org/10.1039/d5dt00742a

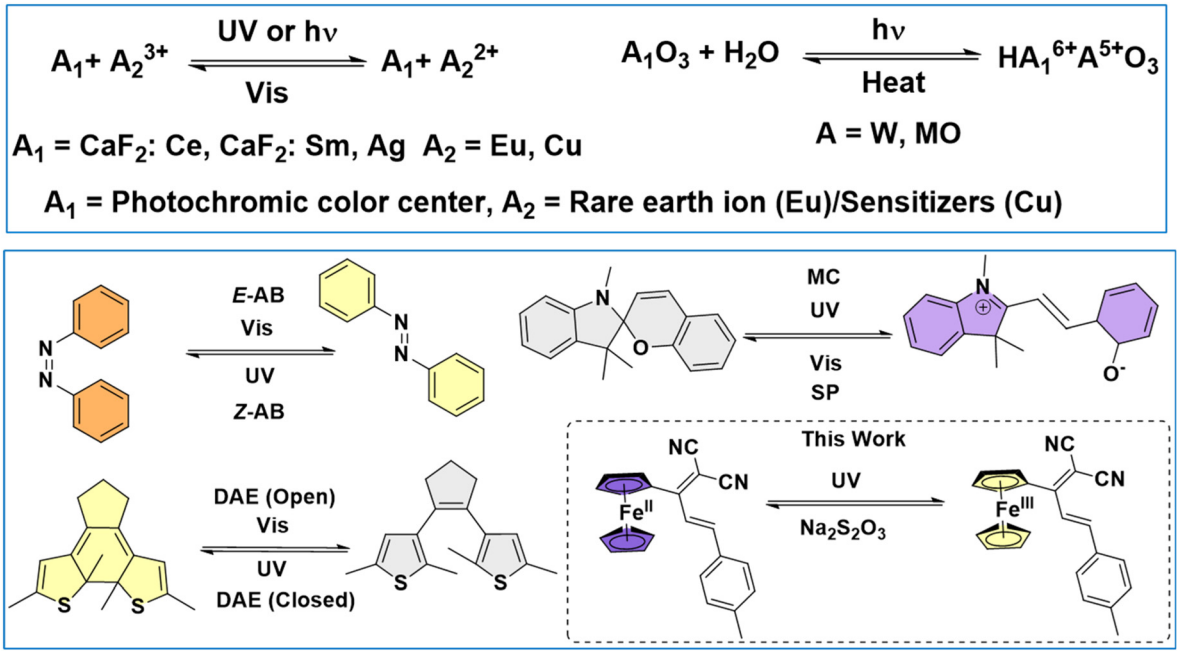

Chart 1 Reported organic and inorganic photochromic materials.

strong visible light absorption. $\mathbf{M_1}$–$\mathbf{M_3}$, upon exposure to UV light, undergo Fc → Fc^+ transformation, leading to high-contrast visual colour changes from blue, yellow and green to yellow, purple and yellow, respectively. Moreover, $\mathbf{M_2}$ also exhibits a turn-on fluorescence upon photoirradiation. The transformation is reversible *via* chemical/electrochemical reduction.

Results and discussion

The synthesis of the target compounds ($\mathbf{M_1}$–$\mathbf{M_3}$) has been achieved by Knoevenagel condensation of dicyanovinylmethyl Fc (**Fc-d**) with respective aromatic aldehydes in the presence of piperidine in ethanol solvent under reflux conditions for 12 hours in moderate to good yields (Scheme 1). The synthesis of $\mathbf{M_1}$ and $\mathbf{M_2}$ was reported earlier,[31] while $\mathbf{M_3}$ was synthesized as part of this study.

To understand the structural and electronic properties of $\mathbf{M_1}$–$\mathbf{M_3}$, geometry optimization has been performed using density functional theory (DFT) (B3LYP/6-31G(d)). The molecules present non-planar structural features, with the dihedral angle between the ferrocene and the dicyanovinylene (dcv) unit being approximately 30–40°.[31] The HOMOs of $\mathbf{M_1}$ and $\mathbf{M_3}$ are in the **Fc** moiety, while the LUMOs are distributed in the

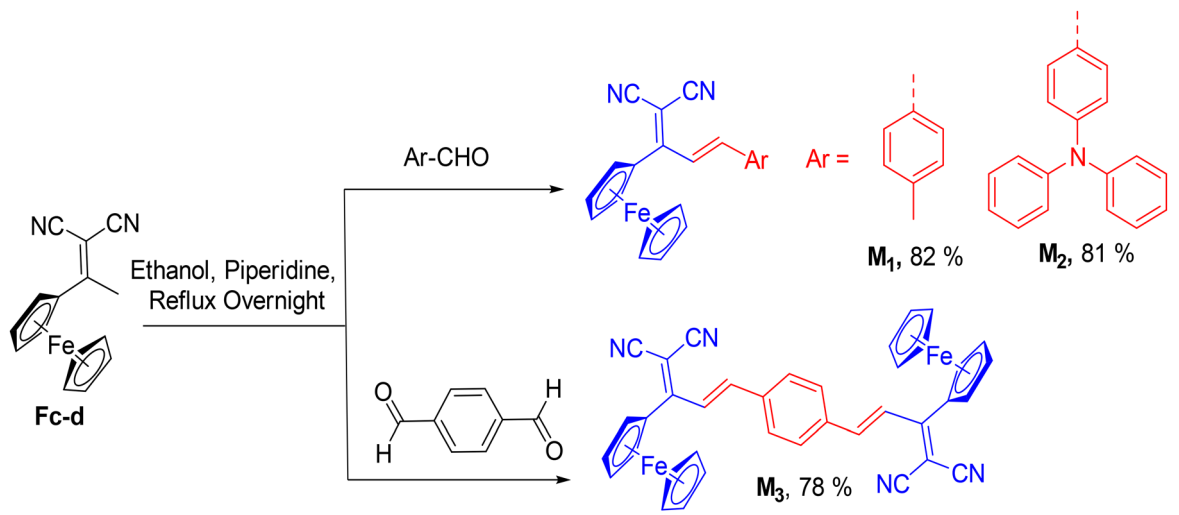

Scheme 1 Synthesis of Fc-based aryl dicyanovinylenes ($\mathbf{M_1}$–$\mathbf{M_3}$).

dcv moiety, indicating strong D–A interactions between the Fc and dcv unit. However, for $\mathbf{M_2}$, the HOMO is located on the triphenylamine (TPA) unit, and the LUMO is localized on the dcv unit. The HOMO/LUMO energies of $\mathbf{M_1}$–$\mathbf{M_3}$ are −5.68/−2.73, −5.30/−2.56 and −5.86/−3.34 eV, with bandgaps of 2.95, 2.74 and 2.62 eV, respectively. The low LUMO and the lower bandgap of $\mathbf{M_3}$ *vs.* $\mathbf{M_1}$ and $\mathbf{M_2}$ are rationalized by the increased electron-accepting strength of dcv (Fig. 1a).

Electrochemical properties of $\mathbf{M_1}$–$\mathbf{M_3}$ have been studied using cyclic voltammetry, with a glassy carbon disk as a working electrode, a Pt wire auxiliary electrode, and an Ag/AgCl reference electrode in a 0.1 M TBAP electrolyte. $\mathbf{M_1}$–$\mathbf{M_3}$

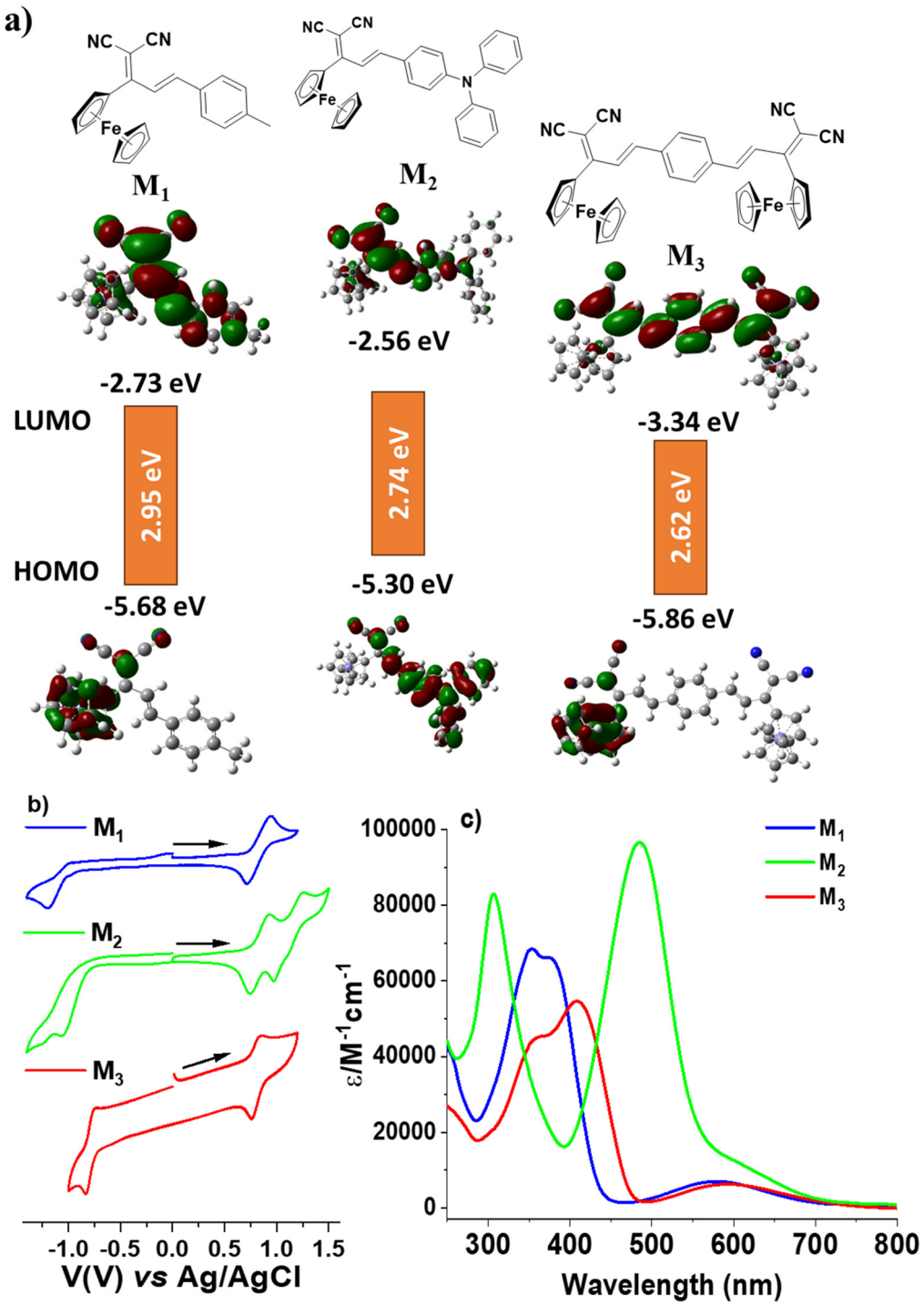

Fig. 1 (a) DFT optimized frontier molecular orbitals and HOMO and LUMO energy diagrams of $\mathbf{M_1}$–$\mathbf{M_3}$. (b) Cyclic voltammograms of $\mathbf{M_1}$–$\mathbf{M_3}$ recorded in 0.1 M TBAP dichloromethane solution at a scan rate of 50 mV s^{-1}. (c) Absorption spectra of $\mathbf{M_1}$–$\mathbf{M_3}$ recorded in CH_2Cl_2 (1×10^{-5} M).

exhibited one reversible oxidation wave in the ~0.8 V (*vs.* Ag/AgCl) range, corresponding to Fc oxidation, and $\mathbf{M_2}$ exhibited an additional oxidation wave at 1.1 V, corresponding to TPA oxidation. On the other hand, all the compounds showed one reversible reduction wave in the range of −0.8 to −1.0 V, corresponding to dcv reduction (Fig. 1b & Fig. S1†). $\mathbf{M_3}$ shows an easier reduction by 0.3 V than $\mathbf{M_1}$ and $\mathbf{M_2}$ due to its electron-deficient nature. The HOMO/LUMO and bandgaps of $\mathbf{M_1}$–$\mathbf{M_3}$ have been evaluated to be −5.0/−3.1, −5.1/−3.2, and −5.2/−3.6 and 1.9/1.9/1.6, matching well with the DFT deduced data (Fig. 1a and b).

The absorption properties of $\mathbf{M_1}$–$\mathbf{M_3}$ have been studied in dilute dichloromethane solution. The compounds showed two absorption bands: a high energy transition in the range of 362–485 nm (ε = 66 000, 95 500, 54 400 M^{-1} cm^{-1}, respectively), corresponding to the π–π* transition and a low energy transition around 590–600 nm (ε = 6500, 12 350, 6650 M^{-1} cm^{-1}, respectively), corresponding to intramolecular charge transfer (ICT) from Fc to the dcv unit (Fig. 1c). However, for $\mathbf{M_2}$, the ICT band was submerged in the strong π–π* transition and appears as a weak shoulder band. $\mathbf{M_2}$ and $\mathbf{M_3}$ *vs.* $\mathbf{M_1}$ exhibit a 128 and 45 nm redshift in the π–π* transition due to increased D–A interactions and extended π-delocalization.

Photochromism

The photochromic behaviour of $\mathbf{M_1}$–$\mathbf{M_3}$ has been studied in dichloromethane at room temperature. Upon irradiation with UV light (254 nm), the colours of $\mathbf{M_1}$–$\mathbf{M_3}$ have been changed from blue, yellow, and green to yellow, purple, and yellow, which is associated with apparent changes in the absorption spectra. The ICT band (~590–600 nm) has disappeared for all three compounds, and new bands at 450 nm for $\mathbf{M_1}$, 606 nm for $\mathbf{M_2}$ and 480 nm for $\mathbf{M_3}$ appeared. Defined isosbestic points at 498 nm for $\mathbf{M_1}$, 540 nm for $\mathbf{M_2}$ and 520 nm for $\mathbf{M_3}$ imply a clean photo-transformation. Thus, $\mathbf{M_1}$ and $\mathbf{M_3}$ show negative photochromism (where the absorption shifts toward the blue region) while $\mathbf{M_2}$ shows positive photochromism (where the absorption shifts toward the red region). This indicates that

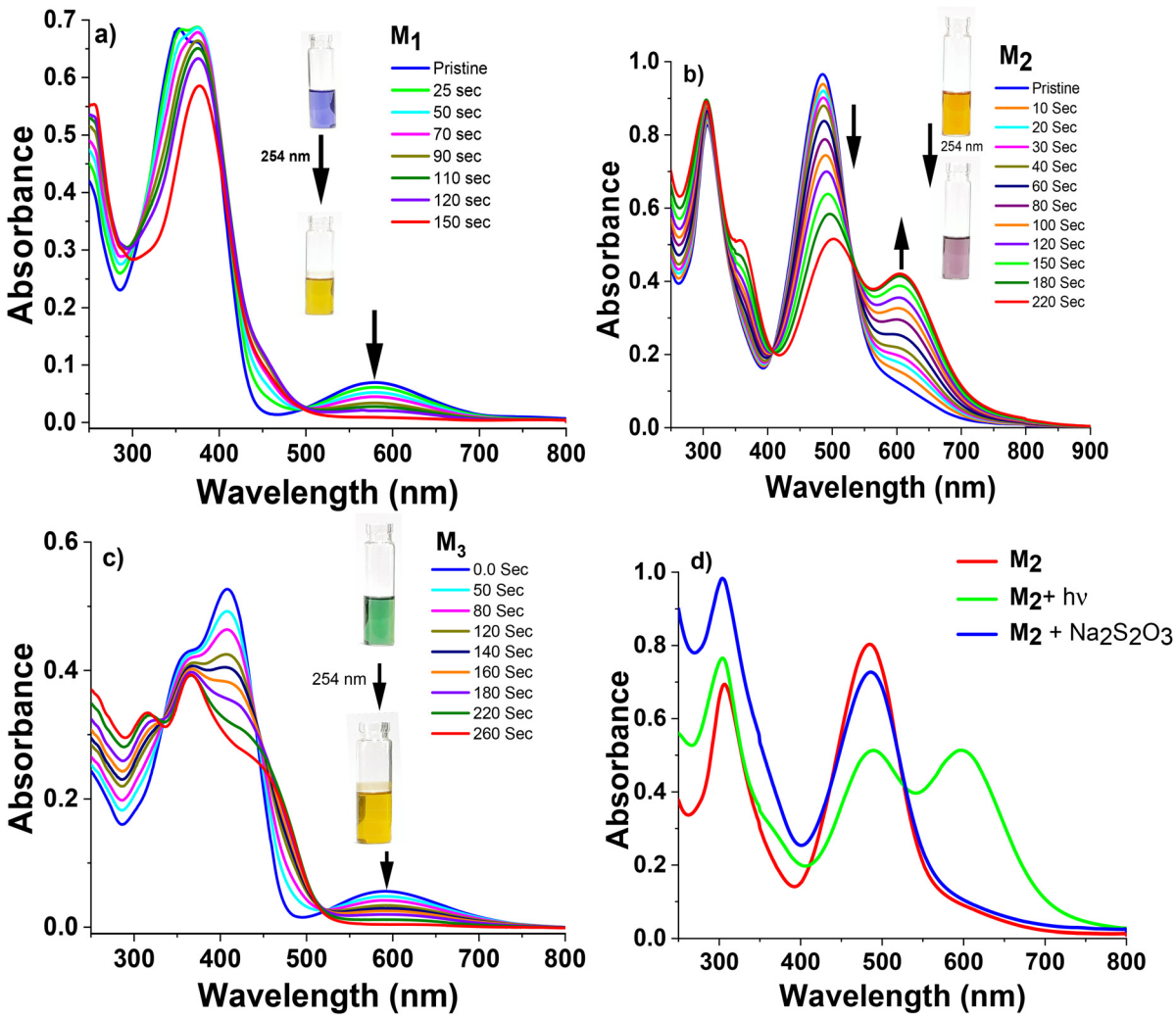

Fig. 2 UV/vis spectral changes of (a) $\mathbf{M_1}$, (b) $\mathbf{M_2}$, and (c) $\mathbf{M_3}$, upon irradiation with 254 nm UV light in CH_2Cl_2. (d) Chemical reversibility of $\mathbf{M_2}$.

the electronic properties of the substituents play a crucial role in tuning the photochromic properties of these compounds. $\mathbf{M_1}$ and $\mathbf{M_3}$, having neutral phenyl substituents, exhibited a negative photochromism with a blue shift in the absorption by quenching the ICT band (ferrocene → DCV). On the other hand, $\mathbf{M_2}$ with a strong electron-donating TPA substituent triggers new charge transfer interactions with DCV after the photo-oxidation of ferrocene. The transformation was found to be quick and completed within 150 s (Fig. 2a–c).

A similar observation was made when $\mathbf{M_1}$–$\mathbf{M_3}$ were subjected to electrochemical oxidation with a potential of 1 V or chemical oxidation with iron perchlorate (Fig. S2†).

The colour and absorption spectral changes have also been the same as the photoinduced transformations. Thus, we speculated that the photo-transformation of $\mathbf{M_1}$–$\mathbf{M_3}$ is due to the oxidation of Fc (Fe^{2+}) to Fc^+ (Fe^{3+}). In the presence of UV light, a photoinduced electron transfer from Fc to CH_2Cl_2 (electron-accepting solvent) may occur, forming Fc^+ (Fe^{3+}) and dichloromethyl anions ($CH_2Cl_2^-$) (Scheme 2).[32,33] To test our hypothesis, we also tested the photochromism of $\mathbf{M_1}$ in CCl_4 (electron-accepting) and toluene (electron-non-accepting) solvents. The CCl_4 solutions exhibited a colour change like the CH_2Cl_2 solution, while no change was observed in the toluene solution (Fig. S3†), indicating that the solvent accepts the electrons from the Fc unit. To further establish that the Fc is oxidizing to Fc^+, nuclear magnetic resonance spectroscopy (NMR), electron paramagnetic resonance spectroscopy (EPR), and Fourier transformation infrared spectroscopy (FT-IR) studies have been carried out on the photo-irradiated system. The NMR spectra of $\mathbf{M_1}$ exhibited a broadening of all the aromatic proton signals upon light irradiation, indicating the paramagnetic nature of the light-irradiated system (Fig. 3a).[34,35]

$$2Fc + CH_2Cl_2 \longrightarrow 2Fc^+ + [\,CH_2Cl_2^{2-} \longrightarrow CH_2Cl^- \longrightarrow :CH_2 + Cl^-\,] + Cl^-$$

Scheme 2 The electron transfer mechanism between Fc and CH_2Cl_2.

In EPR, the photo-transformed product shows a strong EPR signal with a *g*-value of 4.5597, further confirming that the photo-transformed product is paramagnetic and corresponds to the formation of ferricenium ions. On the other hand, no signal was observed for the pristine sample. Moreover, the chemically oxidized sample also showed a similar EPR signal with a matching *g*-value of 4.9490 (Fig. 3b). It is important to note that the *g*-values in the range of 4.5 clearly demonstrate the presence of a metal-based electron, not the organic radical, providing evidence for oxidizing Fe(II) in ferrocene to Fe(III). The FT-IR analysis revealed that the C–C stretching frequency of Fc after light irradiation has shifted from 1440 cm^{-1} to 1720 cm^{-1} due to the oxidation of Fe^{2+} to Fe^{3+}. On the other hand, all the remaining signals corresponding to aryl dicyanovinylene remain unchanged (Fig. 3c & Fig. S4, S5†).

The reversibility of the photo-transformation of $\mathbf{M_1}$–$\mathbf{M_3}$ has been achieved by chemical or electrochemical reduction. Reducing the potential to −1 V or treating the solutions with sodium thiosulphate restored their initial colours and the absorption spectra (Fig. 2d & Fig. S6†). Interestingly, $\mathbf{M_2}$ exhibits turn-on fluorescence upon light irradiation (Fig. 4a) and chemical oxidation (Fig. 4b), with a strong emission signal appearing in the red region (λ_{max} = 675 nm) and reaching its maxima after 200 s. This is attributed to the quenching of the intramolecular charge transfer from ferrocene to dicyanovinylene, while the TPA to dicyanovinylene D–A interaction becomes active.

The signal is broad and spans from 520 to 860 nm and thus exhibits the fluorescence colour of light green instead of the typical red of NIR-emissive systems. The fluorescence quantum yields of the solution have been found to be 4%, which is moderately high for the compounds that show near-IR emission (Fig. 4).

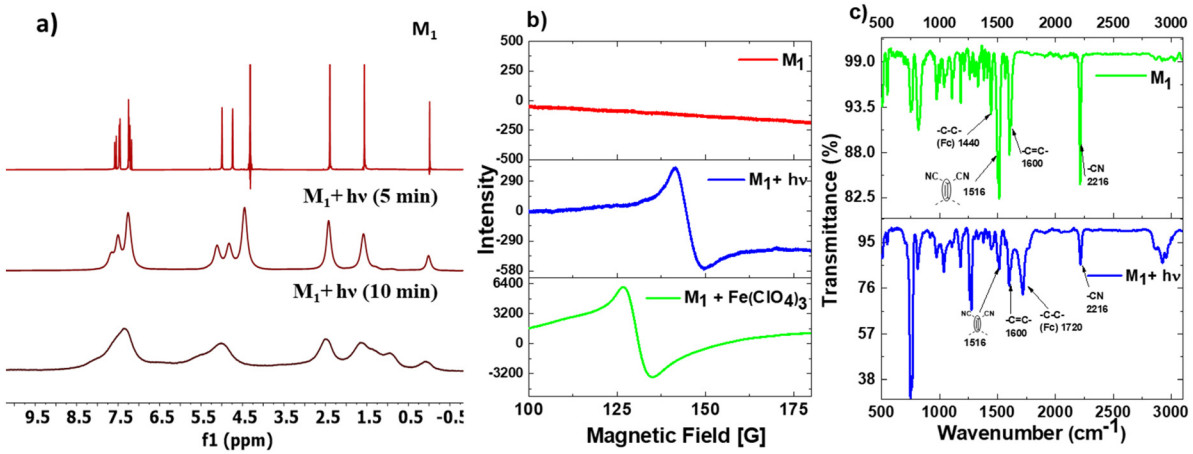

Fig. 3 (a) ^{1}H NMR spectra (400 MHz, $CDCl_3$) of $\mathbf{M_1}$ upon UV light irradiation (top: pristine, middle and bottom: after light exposure); (b) EPR spectra of $\mathbf{M_1}$ before and after irradiation with UV light and chemical oxidation using $Fe(ClO_4)_3$ (1 eq.); and (c) FT-IR spectra of $\mathbf{M_1}$ before and after irradiation with UV light.

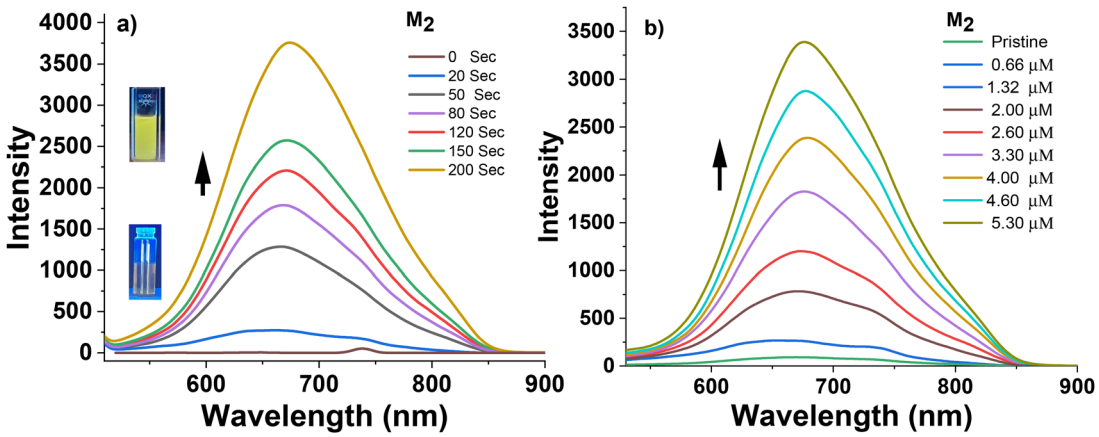

Fig. 4 Emission traces of M_2 (a) after irradiation with a 254 nm lamp and (b) after chemical oxidation using Fe $(ClO_4)_3$ measured in CH_2Cl_2 (1×10^{-4}).

Conclusion

We developed ferrocene-aryldicyanovinylene systems *via* the Knoevenagel condensation of methyl cyanovinylene ferrocene with different aromatic aldehydes (**M_1**–**M_3**). The compounds possess strong intramolecular charge transfer interactions, leading to intense visible light absorption. The systems exhibit photochromism by changing from blue, yellow, and green to yellow, purple, and yellow when irradiated with ultraviolet light, relying on ferrocene's redox switching. In addition, **M_2** also shows photoinduced turn-on fluorescence. These systems represent the first photochromic ferrocene compounds. The work reported here could pave the way for developing functional photochromic materials that can enjoy the benefits of both organic and inorganic systems.

Experimental section

All the chemicals, including ferrocene (98%), *p*-tolualdehyde (98), 4-(diphenylamino) benzaldehyde (96%), terephthalaldehyde (98%), aluminium chloride anhydrous (98%), acetyl chloride (98%) and solvent, were purchased from Sigma-Aldrich, SRL, Loba, TCI-India and used without further purification. ^{1}H NMR (400 MHz), ^{13}C NMR (101 MHz), structural assignments were made with additional information from gCOSY experiments spectra were recorded in deuterated solvent, on a Jeol Resonance ECZ-400R spectrometer. *J* values are expressed in Hz and quoted chemical shifts are in ppm downfield from the tetramethylsilane (TMS) reference using the residual protonated solvents as the internal standard. The signals have been designated as follows: s (singlet), d (doublet), t (triplet), and m (multiplet). Ultraviolet–visible (UV-Vis) absorption spectra were recorded with an Agilent Cary 5000 UV-Vis-NIR spectrophotometer in a 1 cm quartz cell. Fluorescence measurements were carried out on a PerkinElmer FL6500 spectrometer in a 1 cm quartz cell. Density functional theory calculations of the molecular structures (in the gas phase) and the molecular orbital energies were carried out at the B3LYP/6-31G(d) level as implemented in Gaussian 16. The figures were generated with GaussView 6.0. Redox potentials were referenced to ferrocene (Fc/Fc^+). HOMOs were calculated using the equation HOMO = −(4.8 + oxd potential), and LUMOs were determined using LUMO = −(4.8 + redn potential).

Cyclic voltammetry

Electrochemical studies were performed using Gamry INTERFACE 1010 31184 in a three-electrode system by using a Pt wire as a counter electrode, Ag/AgCl as a reference electrode and a glassy carbon disk as a working electrode (3 mm, the surface area of the electrode is 1 cm^2), at room temperature. HPLC grade dichloromethane was used as a solvent with (0.1 M) tetrabutylammonium perchlorate (TBAP) as a supporting electrolyte, and the concentration of the redox species (**M_1**–**M_3**) used was ~1 M. Finally, the redox potentials were modified with reference to the ferrocene (Fc/Fc^+). The scan rate was maintained at 50 mV s^{-1} for all the measurements. All solutions were purged with nitrogen gas using the balloon and needle method before the measurement. In this cyclic voltammetry experiment, the initial potential was set to 0.0 V, and the scan proceeded in the positive (oxidative) direction with a switching potential of 1 V, followed by reversal in the negative (reductive) direction with a switching potential of −1.1 V, and finally back to 0.0 V. This setup allows observation of both oxidation and reduction processes in the redox couple.

Spectroelectrochemical measurements

Spectroelectrochemical measurements were carried out in an electrochemical workstation, Gamry INTERFACE 1010 31184. The changes in the optical absorption in response to electric potential were monitored in a custom-made cell, consisting of a Pt 80 mesh as the working electrode, a 6 mm × 7 mm Pt wire as the counter electrode and Ag/AgCl as the reference electrode. A dichloromethane solution containing the compounds

M_1–M_3 and 0.1 M TBAP as the supporting electrolyte was fed into the spectroelectrochemical cell for the measurements.

General procedure of M_1–M_3

In a 25 mL round-bottom flask, compound **Fc-d** (0.36 mmol), aromatic aldehyde (0.36 mmol) and catalytic amounts of piperidine were added and mixed with 10 mL of ethanol. The flask was heated to reflux for 12 hours. At the end of the time, the reaction mixture was brought to room temperature and poured into water. The resultant solid was filtered and purified by silica gel column chromatography with dichloromethane/petroleum ether (1/1, v/v) as an eluent.

(*E*)-2-(1-Ferrocenyl-3-(*p*-tolyl)allylidene)malononitrile (M_1).

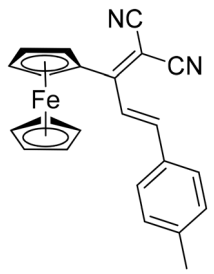

Blue solid (82%), HRMS (QTOF): *m*/*z* calcd for $C_{23}H_{18}FeN_2$ ([M +]): 378.0819; found *m*/*z*: 378.0795; ^{1}H NMR (400 MHz, $CDCl_3$) δ 7.58 (d, $^3J_{H–H}$ = 15.9 Hz, 1H), 7.47 (d, $^3J_{H–H}$ = 7.9 Hz, 2H), 7.24 (d, $^3J_{H–H}$ = 8.0 Hz, 2H), 7.20 (d, $^3J_{H–H}$ = 15.9 Hz, 1H), 5.01 (t, $^3J_{H–H}$, 2.0 Hz, 2H), 4.75 (t, $^3J_{H–H}$, 2.0 Hz, 2H), 4.33 (s, 5H), 2.41 (s, 3H). $\{^1H\}^{13}$C NMR (101 MHz, $CDCl_3$) δ 172.51, 144.55, 141.62, 132.18, 130.04, 128.24, 123.52, 115.98, 115.21, 74.97, 73.09, 71.93, 71.45, 21.67.

(*E*)-2-(3-(4-(Diphenylamino)phenyl)-1-ferrocenyl-allylidene) malononitrile (M_2).

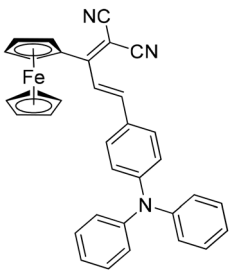

Orange solid (81%), HRMS (QTOF): *m*/*z* calcd for $C_{34}H_{25}FeN_3$ ([M + H]): 532.1471; found *m*/*z*: 532.1446; ^{1}H NMR (400 MHz, $CDCl_3$) δ 7.57 (d, $^3J_{H–H}$ = 15.8 Hz, 1H), 7.42 (d, $^3J_{H–H}$ = 8.8 Hz, 2H), 7.34–7.29 (m, 4H), 7.16–7.10 (m, 7H), 7.02 (d, $^3J_{H–H}$ = 8.8 Hz, 2H), 4.98 (t, $^3J_{H–H}$ = 2.0 Hz, 2H), 4.72 (t, $^3J_{H–H}$, 2.0 Hz, 2H), 4.31 (s, 5H). $\{^1H\}^{13}$C NMR (101 MHz, $CDCl_3$) δ 172.09, 150.58, 146.59, 144.49, 129.63, 129.56, 127.57, 125.69, 124.51, 121.78, 121.36, 116.26, 115.50, 73.87, 72.64, 71.84, 71.28.

2,2′-((2*E*,2′*E*)-1,4-Phenylenebis(1-ferrocene-2-en-3-yl-1-ylidene)dimalononitrile (M_3).

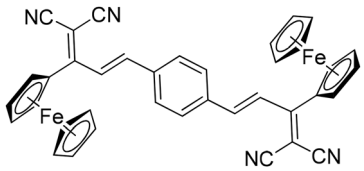

Green solid (78%), ^{1}H NMR (400 MHz, $CDCl_3$), HRMS (QTOF): *m*/*z* calcd for $C_{38}H_{26}Fe_2N_4$ [(M+)]: 650.0856; found *m*/*z*: 650.0844; δ 7.62 (s, 4H), 7.55 (d, *J* = 16.0 Hz, 2H), 7.30 (d, *J* = 16.0 Hz, 2H), 5.05–5.00 (m, 4H), 4.82–4.77 (m, 4H), 4.35 (s, 10H). ^{13}C NMR (101 MHz, $CDCl_3$) δ 172.04, 142.70, 136.94, 128.82, 125.89, 115.72, 77.30, 73.44, 71.87, 71.52.

Data availability

The supporting data for this article have been included in the ESI.†

Conflicts of interest

There are no conflicts to declare.

Acknowledgements

Rajeswara Rao thanks SERB, India, and IIT Dharwad for partially supporting this research through a Core Research Grant (CRG/2023/002129). The authors are grateful to the Sophisticated Central Instrumentation Facility (SCIF), IIT Dharwad, and all its staff members for letting them use the facilities and assisting them with the material characterization studies.

References

1 O. Bertrand and J.-F. Gohy, *Polym. Chem.*, 2016, **8**, 52–73.
2 B. Du, Y. He, M. Shen, Z. Hu, W. Fu, J. Zou, R. Huang and T. Yu, *J. Polym. Sci.*, 2024, **62**, 4809–4834.
3 B. Dutta, S. Datta and M. H. Mir, *Chem. Commun.*, 2024, **60**, 9149–9162.
4 M. Morimoto and M. Irie, *Chem. Commun.*, 2005, 3895–3905.
5 H. Dürr and H. Bouas-Laurent, *Photochromism: Molecules and Systems*, Elsevier, 2003.
6 G. P. Smith, *J. Mater. Sci.*, 1967, **2**, 139–152.
7 M. Irie, *Chem. Rev.*, 2000, **100**, 1683–1684.
8 M. Irie, T. Fukaminato, K. Matsuda and S. Kobatake, *Chem. Rev.*, 2014, **114**, 12174–12277.
9 A. Szukalski, A. Korbut, K. Zieniewicz and S. Zielińska, *J. Phys. Chem. B*, 2021, **125**, 13565–13574.
10 J. Zhang, J. Wang and H. Tian, *Mater. Horiz.*, 2014, **1**, 169–184.

11 Z. L. Pianowski, *Chem. – Eur. J.*, 2019, **25**, 5128–5144.
12 A.-L. Leistner and Z. L. Pianowski, *Eur. J. Org. Chem.*, 2022, **2022**, e202101271.
13 X.-N. Li, H. Xu, L. Huang, Y. Shen, M.-J. Li and H. Zhang, *Dyes Pigm.*, 2023, **213**, 111151.
14 H. Tian and S. Wang, *Chem. Commun.*, 2007, 781–792.
15 Q. Zhou, X. Zhang, L. Ning, Y. Song, Y. Wang, J. Feng, Q. Gong and Y. Huang, *J. Mater. Chem. C*, 2024, **12**, 18991–19016.
16 B. Roubinet, M. Weber, H. Shojaei, M. Bates, M. L. Bossi, V. N. Belov, M. Irie and S. W. Hell, *J. Am. Chem. Soc.*, 2017, **139**, 6611–6620.
17 M. M. Lerch, M. J. Hansen, G. M. van Dam, W. Szymanski and B. L. Feringa, *Angew. Chem., Int. Ed.*, 2016, **55**, 10978–10999.
18 J. Broichhagen, J. A. Frank and D. Trauner, *Acc. Chem. Res.*, 2015, **48**, 1947–1960.
19 J. Du, Z. Yang, H. Lin and D. Poelman, *Responsive Mater.*, 2024, **2**, e20240004.
20 Y. Wakayama, R. Hayakawa, K. Higashiguchi and K. Matsuda, *J. Mater. Chem. C*, 2020, **8**, 10956–10974.
21 S. Chatterjee, S. Molla, J. Ahmed and S. Bandyopadhyay, *Chem. Commun.*, 2023, **59**, 12685–12698.
22 Z. Wu, Q. Wang, P. Li, B. Fang and M. Yin, *J. Mater. Chem. C*, 2021, **9**, 6290–6296.
23 k. Heinze and H. Lang, Ferrocene—Beauty and Function, *Organometallics*, 2023, **59**, 12685–12698.
24 P. Štěpnička, *Dalton Trans.*, 2022, **51**, 8085–8102.
25 L. Fabbrizzi, *ChemTexts*, 2020, **6**, 22.
26 C. Ornelas and D. Astruc, *Pharmaceutics*, 2023, **15**, 2044.
27 A. Khan, L. Wang, H. Yu, M. Haroon, R. S. Ullah, A. Nazir, T. Elshaarani, M. Usman, S. Fahad and F. Haq, *Appl. Organomet. Chem.*, 2018, **32**, e4575.
28 X. Xia, H. Yu, L. Wang and Z. ul-Abdin, *RSC Adv.*, 2016, **6**, 105296–105316.
29 R. Chauhan, M. Trivedi, L. Bahadur and A. Kumar, *Chem. – Asian J.*, 2011, **6**, 1525–1532.
30 P. Garra, D. Brunel, G. Noirbent, B. Graff, F. Morlet-Savary, C. Dietlin, V. F. Sidorkin, F. Dumur, D. Duché, D. Gigmes, J.-P. Fouassier and J. Lalevée, *Polym. Chem.*, 2019, **10**, 1431–1441.
31 A. B. Nipate, A. Raj K and R. R. Malakalapalli, *J. Org. Chem.*, 2025, **90**, 557–569.
32 A. Kotsinaris, G. Kyriacou and C.H. Lambrou, *J. Appl. Electrochem.*, 1998, **28**, 613–616.
33 W. Kirmse, *Carbene Chemistry*, Elsevier, 2013. vol. 1.
34 M. Suzuka, N. Hayashi, T. Sekiguchi, K. Sumioka, M. Takata, N. Hayo, H. Ikeda, K. Oyaizu and H. Nishide, *Sci. Rep.*, 2016, **6**(1), 28022.
35 J. Novotny, S. Komorovsky and R. Marek, *Acc. Chem. Res.*, 2024, **57**(10), 1467–1477.